THE AMERICAN SOCIETY OF MECHANICAL ENGINEERS
345 E. 47th St., New York, N.Y. 10017

96-TA-43

Experimental and Numerical Study of Gust and Gust Response in a Rotor/Stator Axial Compressor

Shu-Tzung Hsu[1] **Andrew M. Wo**[2]
Chun-Kai Wu[3]

Institute of Applied Mechanics
National Taiwan University
Taipei 106, Taiwan
Republic of China

ABSTRACT

This paper addresses the gust response on the stator of a rotor/stator axial compressor, by decomposing the response into vortical and potential contributions. Experiments were conducted in a large-scale, low-speed compressor rig, with two axial gap cases - 10% and 30% chord - and at two time-mean loadings. To determine the gust response due to potential contribution, a two-step approach was taken. First, a panel code was used to determine the gust in the mid-gap plane for the rotor/stator configuration. Then, this calculated gust served as an inlet boundary of a Reynolds-averaged Navier-Stokes code for the stator cascade configuration. The vortical contributed gust response was found by subtracting the potential contributed response from the measured response. Results show that the vortical contributed response is largest near the instant when the rotor wake impinges at the stator leading edge. The potential contributed response reaches a maximum when the rotor trailing edge is axially upstream of the stator leading edge. The vortical contributed response dominates for all cases studied.

NOMENCLATURE

C	chord
F	force on the stator
h	circumferential spacing of line vortices in panel method
k	turbulence kinetic energy
M	moment about the mid-chord
Re	Reynolds number based on inlet flow velocity and blade chord
R_t	turbulence Reynolds number ($=\rho k^2/(\mu\varepsilon)$)
S	circumferential blade pitch or length of panel
t, t'	time, the prime implies in the moving frame
u^+	streamwise component of unsteady velocity
w	complex velocity potential
u_i^+	i^{th} harmonic streamwise gust
$\mathbf{V}$	absolute flow velocity vector ($=ui+vj$)
$\mathbf{V}_b$	rotor blade wheel velocity vector
v^+	transverse component of unsteady velocity
W_p	instantaneous relative velocity from potential code
W	instantaneous relative velocity
Z_g	axial gap

Greek Symbols

ε	dissipation rate of turbulence kinetic energy
Φ	mass flow coeficient
ϕ	velocity potential
λ	normalized turbulence length scale
ρ	density of fluid
μ	$1/R_e$
μ_t	eddy viscosity coefficient ($=\rho C_\mu f_\mu k^2/\varepsilon$)

Subscripts

b	blade
g	axial gap
NS	Navier-Stokes calculation
n	direction normal to the chord or to the panel surface
p	potential disturbance
v	vortical disturbance
G	an infinite series of 2D vortices
∞	inlet condition

Headed Quantities

$\bar{}$	time mean
$\sim$	unsteady part, instantaneous minus time mean

1.0 INTRODUCTION

Unsteady force experienced by blades in turbomachines generally arise from two sources: self-excited flow instability and forced

1 Doctoral Student
2 Associate Professor (lead correspondent)
3 Research Assistant

Presented at the 1996 ASME Turbo Asia Conference
November 5–7, 1996 — Jakarta, Indonesia

response. Self-excited instability can lead to blade vibration, or flutter. Forced response can be considered due to vortical and potential effects, with the vortical contribution arises mainly from wake/blade interaction, and the potential contribution from relative motion between blade rows. Disastrous blade failure, such as high-cycle fatigue, can occur when the flow forcing frequency matches the blade natural frequency. Unfortunately, avoidance of all modes that the two frequencies coincide are not feasible within the operating range of an actual machine. Thus it is important to better understand the fundamental mechanics involved, then seek ways to decrease the unsteady blade force. From the stress-cycle diagram, one realizes that a fractional decrease of the unsteady blade loading can substantially increase the blade life.

Many researchers had undertaken studies of gust and gust response in axial turbomachines. A comprehensive review of the subject can be found in AGARD (1987a and 1987b). A summary of recent advances in forced response analyses was provided by Kielb and Chiang (1992). Verdon (1993) also reviewed unsteady aerodynamic methods for turbomachinery aeroelastic and aeroacoustic applications. Numerous excellent calculations of unsteady blade force for rotor/stator or wake/blade configuration include Rai (1987), Lewis and Delaney (1987), Giles (1988, 1990), Rai and Madavan (1990), Korakianitis (1993a, 1993b), Chung and Wo (1995), Valkov and Tan (1995), and others. The work of Valkov and Tan provided exceptional physical insight into the cause of unsteady blade loading due to moving wakes. Experimental studies which focus on the unsteady blade loading include Fleeter et al. (1981), Capece and Fleeter (1987), Gallus et al. (1982), Manwaring and Wisler (1993), and others. The work of Manwaring and Wisler emphasized the importance of properly accounting both vortical and potential contributions to calculate the total unsteady response.

The focus of this work is to address individual contributions of vortical and potential effects on the overall stator gust response. The primary motivation of decomposing into the two contributions is their physical significance. For the rotor/stator configuration under study, the stator experiences a vortical gust response due to impingement and subsequent convection of the rotor wake. The potential response originates from the moving pressure field attached to the rotor blade, as viewed in the stator frame, which results in a periodic disturbance on the stator.

This paper answers the following questions concerning gust response on the stator of the experimental rotor/stator axial compressor, for two axial gaps - 10% and 30% chord - and two time-mean loadings:

- what is the magnitude of the *vortical* contribution to the overall stator gust response?
- what is the magnitude of the *potential* contribution to the overall stator gust response?
- when are the two individual contribution largest within a blade-to-blade period?

The first two questions compare the two contributions, under various geometric and flow conditions. The third question is important since the maximum unsteady response for vortical and potential contributions determine the maximum stress in the blade stress-cycle diagram. The motivation behind these questions is to lay the groundwork for design to reduce the maximum unsteady blade load by beneficial usage of unsteady interactions due to vortical and potential contributions.

To answer the questions stated, the key step is to decompose the stator gust response into vortical and potential contributions. The approach adopted is briefly outlined here. Due to the fact that the rotor/stator experiment cannot isolate the potential contribution alone, a panel code for rotor/stator calculation is needed for this purpose. However, there is great difficulty in calculating the unsteady pressure on the stator surface accurately; vortices shed from the rotor, convect downstream without decay, and can be in close proximity to a stator panel, which cause unphysical changes in the unsteady surface pressure. This is especially difficult to overcome due to close proximity between blade rows, about 30% chord in modern compressors. To circumvent this problem, a two-step approach was taken. First, a panel code was used, for rotor/stator configuration, to determine the gust in the mid-gap plane between blade rows. Second, this potential-contributed gust, plus the time-mean flow, served as an inlet boundary condition for stator alone configuration in a Navier-Stokes calculation, to determine the gust response due to potential contribution. Thus, the Navier-Stokes code merely served as a tool to obtain the potential-contributed gust response. The vortical-contributed gust response was found by subtracting the potential-contributed response from the response measured experimentally. Justification for this approach, and more details, are provided in Section 4.0.

2.0 EXPERIMENTAL SETUP

The experimental compressor is a low-speed, large-scale, one-to-three stage rig, designed after modern compressors, see Fig. 1 and Table 1. Flow enters the compressor through a bell-mouth contraction and into the blade annulus. In this work, IGV/rotor/stator configuration was used. The IGV trailing edge was located at 1.75 chord upstream of the rotor leading edge, to allow for wake dissipation. The blades were designed using controlled diffusion concept of Hobbs and Weingold (1984). Two special features are designed in the rig - the axial gap is variation, from 10% to 30% chord, and the circumferential relative position between rotor blade rows can be adjusted. Only the first feature was used in this work.

The measured stage static pressure rise is shown in Fig. 2, for both 10% and 30% chord axial gaps. The pressure rise obtained is believed to be representative of modern highly loaded blade design. Data show that the pressure rise increases with decreased axial gap except near stall. This general trend agrees with that of Smith (1969). In this work, tests were conducted at near-design loading (Φ= 0.60) and high loading (Φ= 0.53). The compressor achieves a static-to-static efficiency of slightly over 90% for both gap cases.

Instrumentation include measurements of stator surface unsteady pressure, unsteady velocity, time-mean pressure and torque. The unsteady pressure on the stator surface was measured using fast-response pressure transducers (5psid Kulite LQ-125), which were embedded within two blades (due to space constraint) - 10 transducers to measure the suction surface of one blade and 10 on the pressure surface of an adjacent blade. To provide timing information, a photo-sensitive diode was used to sense the passing of a metal protrusion rotating with the shaft, with a timing accuracy of 0.1% of a blade-to-blade period. This signal was used to correct for the phase difference in the stator unsteady pressure measured on two separate blades. The pressure transducer output, as a differential signal, was connected to a low-noise amplifier (Stanford Research SR560). The

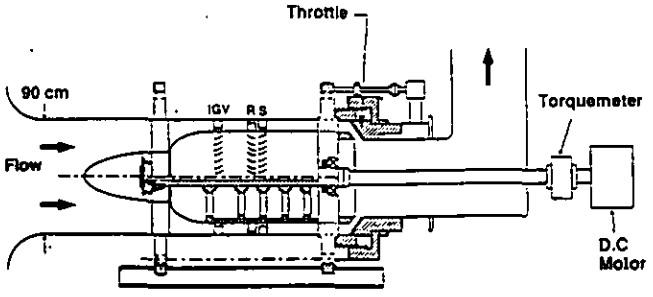

Fig. 1 The experimental compressor in IGV/rotor/stator configuration.

	IGV	Rotor	Stator
Blade Number	60	58	60
Chord (cm), C	6.00	6.00	6.00
Span (cm), S	8.88	8.88	8.88
Solidity	1.415	1.368	1.415
Tip Clearance	2.0%C	2.0%C	2.0%C
Aspect Ratio (S/C)	1.48	1.48	1.48
Trailing Edge Radius (%C)	1.0 %	1.0 %	1.0 %
Stagger (deg.)	6.58 °	-39.50 °	20.67 °
Camber (deg.)	3.2 °	35.0 °	48.0 °
Inlet Angle, β 1 (deg.)*	0.0 °	56.21 °	46.80 °
Exit Angle, β 2 (deg.)*	9.78 °	31.03 °	4.76 °
Diffusion Factor	-	0.407	0.485
Axial Gap	1.75C	10%C & 30%C	
Mass Flow Coefficient	0.53 ~ 0.70		
Rotor Tip Speed (m/s)	49.48		
Working Shaft Speed (RPM)	1050		
Inlet Casing Diameter (cm)	90.0		
Hub/Tip Ratio	0.8		
Reynold's Number at 1050RPM (rotor relative)	1.92×10^5		

* from hot-wire located at mid-gap, mid-pitch, for axial gap of 30% chord.

Table 1 Compressor and blade parameters at design condition.

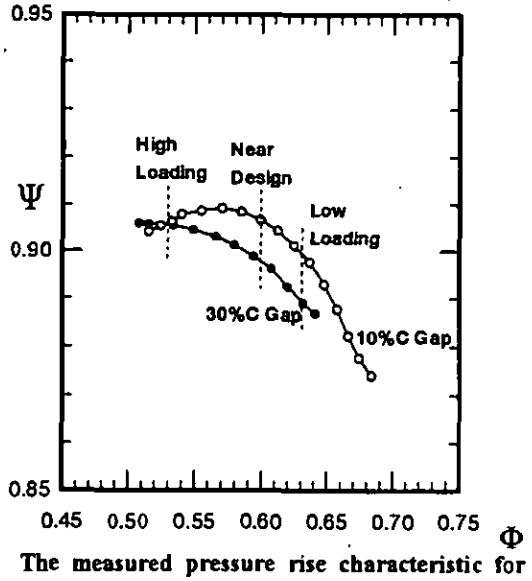

Fig. 2 The measured pressure rise characteristic for axial gap of 10%C and 30%C between blade rows.

amplifier output was sent to a PC-based analog/digital card (National Instrument AT-MIO-16F-5), where 128 data points were acquired in a rotor blade-to-blade period. To preserve the time series, analog filter was not used prior to A/D, but the signal was monitored using a spectrum analyzer (HP 3561A). No high frequency content exists which could aliase the blade-to-blade frequency and its nine higher modes. The digitized signal was Fourier transformed using FFT to extract the first ten modes, and inverse FFT was applied to recover the time series. Extreme care was exercised to sure the phase information was reconstructed correctly.

Unsteady velocity was measured using a 45 degree slanted, miniature hot-wire (TSI 1263A-T1.5) and anemometer system (TSI IFA-100). The slanted hot-wire was calibrated in a wind-tunnel within the range of velocity and flow angles, both yaw and pitch, encountered in the compressor flow field, with an accuracy of 3% in velocity within the wake region. During measurement, the hot-wire probe was rotated, along its axis, in three orientations in order to extracted the three velocity components, using technique primarily adopted from Schmidt and Okiishi (1977). Care was exercised to ensure that the flow angles were within the calibration range for all three orientations, especially within the wake region.The velocity data were acquired similar to that of the surface pressure data described above, except no digital filter was used.

A torquemeter (S. Hinnelstein & Co. model 2904T5-3) was mounted between the D.C. motor and the compressor shaft, thus the efficiency can be calculated. The torque due to the rotating assembly alone, without any blade mounted, was first measured at the working RPM. This torque was subtracted from that measured with the rotor/stator configuration.

3.0 NUMERICAL METHODS

Both Navier-Stokes and potential codes were used in this work. This section briefly describes the calculation methods. More details can be found in Chung (1995), and Chung and Wo (1995).

3.1 Navier-Stokes Calculations.

Calculations were performed using a two-dimensional incompressible Reynolds-averaged Navier-Stokes code written for multi-stage configuration. Governing equations in the blade relative frame are

$$\nabla \cdot \mathbf{u} = 0, \tag{1}$$

$$\frac{\partial \mathbf{u}}{\partial t} + \nabla \cdot \left[(\mathbf{u} - \mathbf{u_b})\mathbf{u} \right] = -\nabla P + \nabla \cdot \left[(\mu + \mu_t)\nabla \mathbf{u} \right], \tag{2}$$

where $\mathbf{u_b}$ is the blade velocity, which equals the rotation speed for the rotor and zero for stator. The modified Launder-Sharma low Reynolds number version of k-ε two-equation model (LS model, Morse 1991), was used to close the above equations via the eddy viscosity coefficient μ_t, which could be written as

$$\frac{\partial k}{\partial t} + \nabla \cdot \left[(\mathbf{u} - \mathbf{u_b})k \right] = \nabla \cdot \left[\left(\mu + \frac{\mu_t}{\sigma_k} \right) \nabla k \right] + G_k - \varepsilon - D, \tag{3}$$

$$\frac{\partial \varepsilon}{\partial t} + \nabla \cdot \left[(\mathbf{u} - \mathbf{u_b})\varepsilon \right] = \nabla \cdot \left[\left(\mu + \frac{\mu_t}{\sigma_\varepsilon} \right) \nabla \varepsilon \right] + C_1 f_{\mu_1} G_k \frac{\varepsilon}{k} - C_2 f_{\mu_2} \frac{\varepsilon^2}{k} + E - F, \tag{4}$$

where $G_k = \mu_t (\partial u_i / \partial x_k)(\partial u_i / \partial x_k + \partial u_k / \partial x_i)$,

$D = 2\mu\left(\partial\sqrt{k}/\partial x_j\right)^2$, $E = 2\mu\mu_t\left(\partial^2 u_i/\partial x_j{}^2\right)^2$, $F = 2\mu\left(\partial\sqrt{\varepsilon}/\partial x_j\right)^2$,

$C_\mu = 0.09$, $C_1 = 1.44$, $C_2 = 1.92$, $\sigma_k = 1.0$, $\sigma_\varepsilon = 1.22$,

$f_\mu = \left[1 - \exp\left(-y^+/A^+\right)\right]^2$, $A^+ = 25$, $f_{\mu_1} = 1.0$,

$f_{\mu_2} = 1 - 0.21875\exp\left(-R_t{}^2/36\right)$. The turbulence Reynolds number is defined as $R_t = \rho k^2/(\mu\varepsilon)$, the wall variable $y^+ = \rho y U_\tau/\mu$, and the wall shear velocity $U_\tau = \sqrt{\tau_w/\rho}$.

Equations (1) to (4), in its conservative form as shown, were solved by the finite volume approach, using essentially the iterative method Semi-Implicit Method for Pressure-Linked Equations (SIMPLE) (Patankar and Spalding 1972). In this work, the non-staggered grid was used, with the computation nodes located at the grid cell center. For time discretization, a Crank-Nicolson-like scheme was used to achieve second-order time accuracy. For space discretization, the convection term was approximated by the QUICK scheme (Leonard 1979), while other terms by the central difference scheme, which made the code formally second-order accurate.

The computational domain is bounded by various boundaries including in-flow and out-flow boundaries - located at 1.5C upstream of the stator leading edge and 1.5C downstream of the rotor trailing edge, respectively - the interface boundary between blade rows, the periodic boundary and the rigid blade surface, as shown in Fig. 3. Each blade row is associated with an body-fitted embedded H-type grid. To check grid independence, two grid sizes were computed (Chung 1995) - 172x78 cells per row, with 108 cells per blade surface, and 258x114 cells per row, with 160 cells per blade surface. The results calculated using the coarse grid was found not to differ significantly from that using the finer grid, thus the coarse grid was used throughout this work.

There is a difference in the rotor-to-stator blade counts between the calculation, which uses a 1:1 count, and the experiment, which is 58:60. However, this difference is not believed to be significant, which corresponds to t/T= 0.033 compared to a typical wake width of t/T= 0.20. Moreover, focus is placed on the stator gust response in this work, thus, for a stationary observer the normalized time T is based on the rotor motion, or the rotor pitch divided by blade speed, for both calculation and experiment. Thus the time t/T= 0.033 does not cause direct phase error, rather indirectly due to slightly modified blade-to-blade flow.

Figure 4 presents a comparison between the wake measured by the hot-wire and the Navier-Stokes calculated gust (prior to decomposition), for both axial gap cases and at two time-mean loadings, with the hot-wire located at the mid-gap and the stator mid-pitch position. Both data and calculation show the same trend that the wake defect decreases with downstream distance, while the wake width increases downstream. The overall agreement is considered acceptable, taking into account that at 5%C to 15%C behind the rotor trailing edge, where results in Fig. 4 were taken, the wake is still believed to posses the characteristics of that of a near-wake. Close scrutiny of the calculated wake, however, reveal that the wake width is less than that measured for all cases considered.

Comparison of the measured unsteady force on the stator with calculation is shown in Fig. 5, for axial gap of 30%C. Again the overall trend is acceptable, but the amplitude and fine features of the

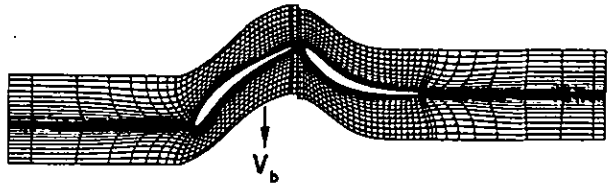

Fig. 3 Computation grid used in the Navier-Stokes calculation (1/4 density shown for clarity).

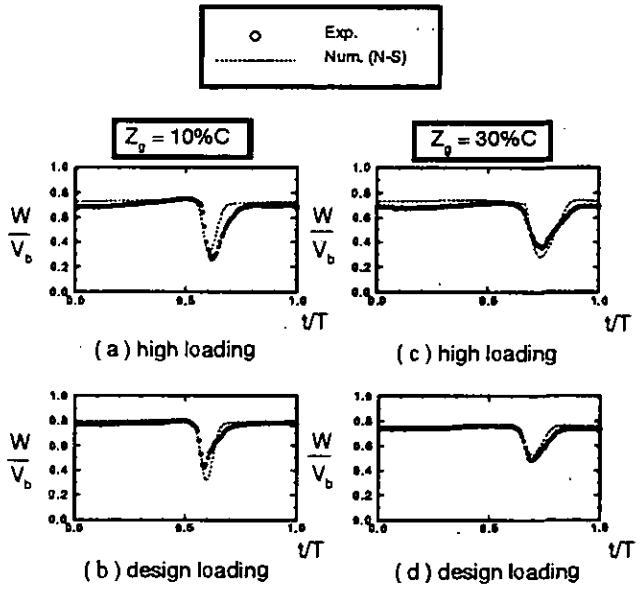

Fig. 4 Comparison of hot-wire measurement, located at mid-gap and stator mid-pitch, with Navier-Stokes calculated disturbance, for 10%C and 30%C axial gaps and two loadings.

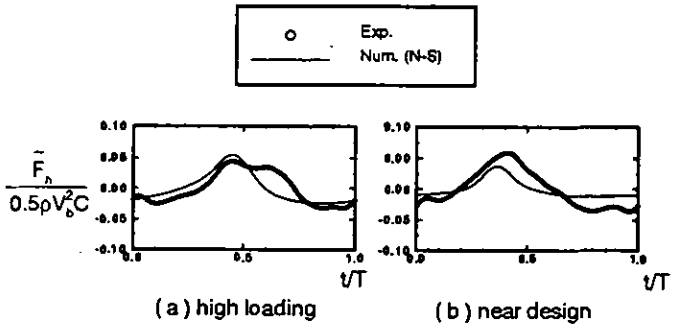

Fig. 5 Comparison between experimental data and Navier-Stokes calculated unsteady force, prior to decomposition.

unsteady force signature are not very well predicted. The issue of turbulence modeling, which is believed to be accountable for the discrepancy, is known to be thorny for a wake within the gap region, during the process of wake impingement on the stator surface, and subsequent convect within the blade passage.

3.2 Panel Method Calculations.

In this work, a panel code was used to calculate the potential-contributed gust in the mid-gap plane of the rotor/stator configuration. The essential elements of the method is largely based on a code listing by Kuethe and Chow (1986), with modification to account for multiple cascade geometry in an unsteady flow. Some basics and details on the modification follow.

The panel method solves for the velocity potential via the governing equation $\nabla^2\phi = 0$. The boundary condition on the blade surface is $\partial\phi/\partial n = \mathbf{u}_b \cdot \mathbf{n}$, where $\mathbf{u}_b$ is the blade surface velocity. Also, vortices were shed into the flow at each time instant to satisfy the Kelvin's theorem, or $D\Gamma/Dt = 0$. The Kutta condition was satisfied by enforcing zero vorticity strength at the trailing edge. The criteria by Basu and Hancock (1978) was used to determine from which surface at the trailing edge vortices were shed into the flow.

Vortex panel method was used to solve this unsteady potential flow field, with vorticity distribution of linearly varying strength located on each panel. A total of 201 panels are used on each blade. To account for the multiple cascade configuration, an infinite number of 2D vortices were distributed circumferentially for each row of cascade, and separated by a blade pitch h, with the strength, G. The complex velocity potential (Lamb 1945) due to these vortices is

$$w_\Gamma(z) = i\Gamma ln\left[sin\frac{-i\pi(z - z_\Gamma)}{h}\right], \qquad (5)$$

with each vortex located at $Z_\Gamma = inh$, where $i = \sqrt{-1}$, n=1 to ∞. From the relationship between the complex velocity and the physical velocity, $dw/dz = u - iv$, the induced velocity due to the vortices can thus be found.

4.0 DECOMPOSITION OF VORTICAL AND POTENTIAL CONTRIBUTION

The key approach in this paper is to decompose the unsteady response on the stator into vortical and potential contributions. For the rotor/stator configuration being considered, this cannot be done by experiment alone, nor by a Navier-Stokes calculation, which, in principle, contains both contributions simultaneously. To wit, one can determine either contribution individually, and subtract this from the total (prior to decomposition) response. This assumes, however, that superposition holds. The Navier-Stokes calculation (the UNSFLO code) by Giles, in Manwaring and Wisler (1993), proved this point definitively. With the inlet boundary condition of a stator cascade calculation based on purely first mode (blade-to-blade) gust, measured in the mid-gap of the GE large-scale compressor rig, the calculated response of the second mode was less than 2% of that of the first mode, which suggested that non-linearity can be neglected. Thus the gust *response*, even though scales with velocity squared, can indeed be linearized, about a non-linear time-mean (Hall and Crawley, 1989). Therefore, superposition for the *gust* based on vortical and potential contributions should also be valid.

In light of the above, the entire gust response decomposition procedure would be straight forward if the panel code could be used to accurately compute the unsteady pressure on the stator surface, for a rotor/stator configuration. The problem arises when shed vortices, as required by Kelvin's theorem, from the rotor are very close to the stator surface panel. Although a mirror-image procedure was used, based on the assumption of perfect reflection, to relocate a vortex that otherwise, if no special arrangement was made, could result in the

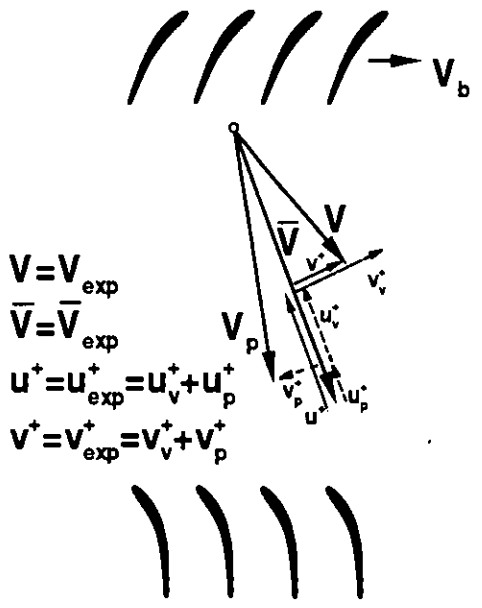

Fig. 6 Vector diagram showing the decomposition of the total gust, for a location within the gap region, into vortical and potential contributions. (Symbols: u^+ = streamwise gust, v^+ = transverse gust. Subscripts: exp = experiment, v = vortical, p = potential.)

vortex penetrating through the panel by the next time increment (Chung 1995), the fact that the reflected vortex is in close proximity of the panel surface causes unphysical changes in the calculated unsteady pressure.

To circumvent this difficulty, a two-step approach was adopted to arrive at the stator gust response due to potential contribution alone. First, the panel code was used to determine the gust in the mid-gap plane between blade rows for rotor/stator configuration. For an observer fixed in the stator frame, the motion of the rotor is equivalent to a moving pressure field, which causes an unsteady flow, or gust, due to changes in fluid acceleration. Second, this potential-contributed gust, plus the time-mean flow, served as an inlet boundary condition in a Navier-Stokes calculation for stator alone configuration. This determines the stator gust response due to potential contribution. Thus, the Navier-Stokes code merely served as a tool to obtain the potential-contributed gust response. The vortical-contributed gust response was found by subtracting the potential-contributed response from the response measured experimentally. The sub-sections following provide further details on the two-steps procedure.

4.1 Gust Decomposition.

Figure 6 illustrates the gust decomposition graphically. Hot-wire measurement, at a fixed location between the blade rows, provides the instantaneous velocity, or V, and the time-mean velocity $\bar{V}$. The total gust (prior to decomposition) is obtained by subtracting $\bar{V}$ from V, and is resolved into streamwise and transverse components, U^+ and V^+ respectively, with the streamwise component parallel to $\bar{V}$. For the same point where the total gust is obtained, a panel calculation for rotor/stator configuration provides the instantaneous velocity, or V_p, at that location. The gust due to

potential contribution, U_p^+ and V_p^+, is obtained by subtracting $\bar{V}$ from V_p, minus the contribution from shed vortices. That is, gust due to vortices shed from the rotor trailing edge is not considered as potential-contributed gust. (Explanations are provided in the following paragraph.) The gust due to vortical contribution, U_v^+ and V_v^+, is obtained by subtracting U_p^+ from U^+ and V_p^+ from V^+. In this procedure it is important to keep the mass flow the same for the panel calculation and the experiment. The entire process presupposes that the actual gust due to potential contribution, not the instantaneous flow, is well represented by that calculated by the panel code. With the time-mean mass flow kept constant, this is believed to be a reasonable assumption, even for the high-loading case since an increase in the wake width would cause the vortical-contributed gust to increase, and not directly affect the potential contributed gust.

Explanation for excluding the contribution of shed vortices from the rotor follows. Gust due to shed vortices, as dictated by the Kelvin's theorem, is viewed as a viscous phenomenon, which arises from the Kutta condition, and should be included in the gust due to vortical contribution. Physically, the shed vortices are embedded in the boundary layer, and cause unsteadiness in the wake. Hence, the shed vortices are indeed a viscous contribution to the gust. In the panel calculation, exclusion of the contribution due to shed vortices is simply not calculating their contributions toward the net unsteady potential function; since the Laplace's equation is linear, this procedure is straightforward.

4.2 Gust Response Decomposition.

With the gust due to potential contribution known, the gust response is calculated using the known gust, plus the time-mean flow, as an inlet boundary condition to the Navier-Stokes code for a stator alone configuration. The vortical contribution to the gust response is simply the potential-contributed response subtracted from the measured response.

The reason that the Navier-Stokes code is not used to obtain the vortical-contributed response lies with its difficulty in resolving the fine features of the unsteady force, as shown in Fig. 5. As mentioned earlier, this is most likely due to the turbulence model used, two-equation k-ϵ, not capturing relevant physics of wake-blade interaction. As for computing the potential-contributed gust response, the Navier-Stokes should have much less difficulty, due to that the velocity gradient for the potential gust, with a length scale, is much less severe than that of the wake, as will be discussed in the following section.

5.0 RESULTS AND DISCUSSIONS

5.1 Unsteady Velocities.

Figures 7a and 7b present the Navier-Stokes calculated unsteady velocity for 10%C and 30%C axial gaps, respectively. (The unsteady velocity here is defined as the instantaneous velocity minus the local time mean.) These plots serve to provide an overall view for the two gust contributions, with the length of a vector represents the strength of the disturbance. The apparent discontinuity in the mid-gap plane, where the slip interface is located, is due to non-uniform grid density in the fixed and moving grids separated by the interface.

It is well-known that potential gust is an important source of flow unsteadiness for close axial gap, e.g. 10%C, and is clearly shown by the blade-to-blade, wave-like structure in Fig. 7a. Perhaps the most

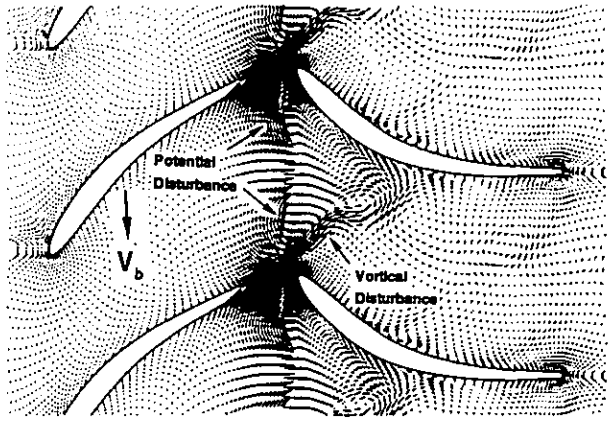

Fig. 7a Unsteady velocity vectors calculated by the Navier-Stokes code for rotor/stator configuration at *10%C* axial gap. Vortical disturbance is due to the wake, and is also present within the stator passage. Potential disturbance is locked to the adjacent moving blades, with the blade pitch as its length scale.

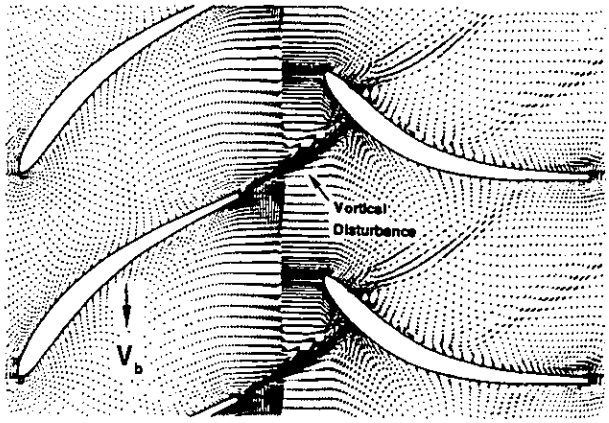

Fig. 7b Unsteady velocity vectors calculated by the Navier-Stokes code for rotor/stator configuration at *30%C* axial gap, where the potential disturbance has essentially vanished.

important nature of this disturbance is that its associated disturbance pressure field is locked to the moving blade as viewed in the fixed frame, and vice versa; Fig. 7a shows the peak of the potential disturbance occurs at the rotor trailing edge. The vortical gust due to the wake is also clearly shown. At 30%C axial gap, Fig. 7b shows only vortical gust is present. Chung and Wo (1995), and others, have shown that the potential disturbance indeed decays exponentially.

5.2 Vortical and Potential Disturbances.

To illustrate the vortical and potential gusts experimentally, hot-wire measurement was made at locations indicated in Fig. 8a - Points A, B, C, D, and M. The Point B was located axially upstream of the stator leading edge. Points A and C were placed 0.1 stator-pitch circumferentially on either side of the Point B. The Point D was located as closed to the stator surface as possible, 2mm from the surface and 3mm chordwise (or 5%C) position, where a surface-mounted Kulite pressure transducer was closest to the leading edge.

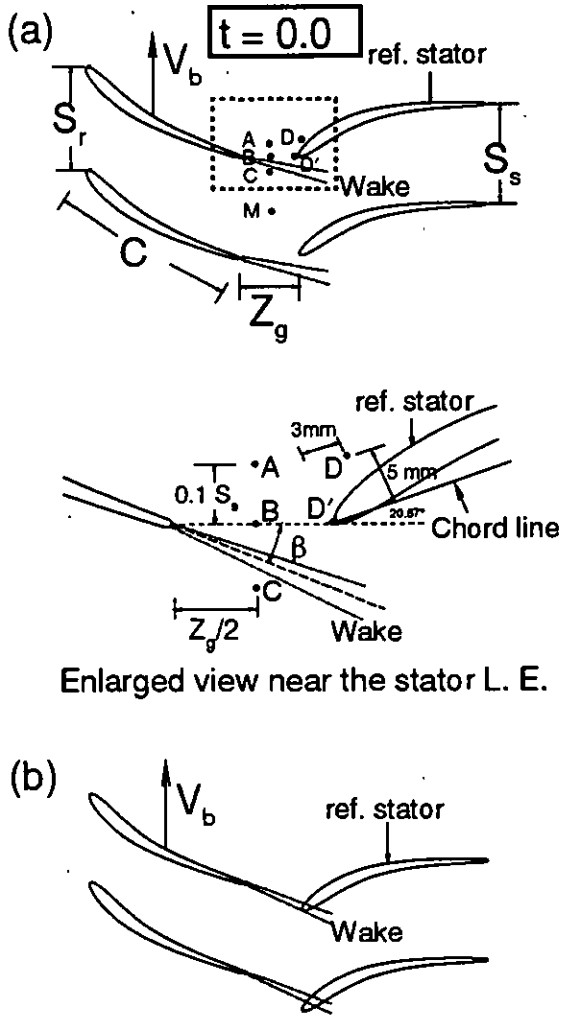

Fig. 8 **A sketch of the relative position between the rotor and the stator. Figure 8a shows the time when the rotor trailing edge is axially upstream of the stator leading edge, at time t = 0.0. Also shown are hot-wire locations for gust measurement, with the view enlarged for clarity. Figure 8b shows the time when the rotor wake arrives at the stator leading edge.**

Hot-wire data at Point D, along with the associated pressure transducer, serve to detect the wake when it is in close proximity to the stator leading edge. As will be clear shown, the stator leading edge is an important location for consideration of the vortical gust response. Point M was placed at the mid-gap and stator mid-pitch location, and resulted in the gust free from influence of the stator. Greater details of these locations are shown in the enlarged view.

Figures 8a and 8b also serve to illustrate the definition of time used throughout this work. The time t = 0.0 is when a rotor trailing edge is axially forward of the leading edge of the reference stator, where the unsteady force and moment are considered.Figure 8b sketches the time instant when the rotor wake arrives at the stator leading edge.

Figure 9 presents the total (prior to decomposition), vortical and

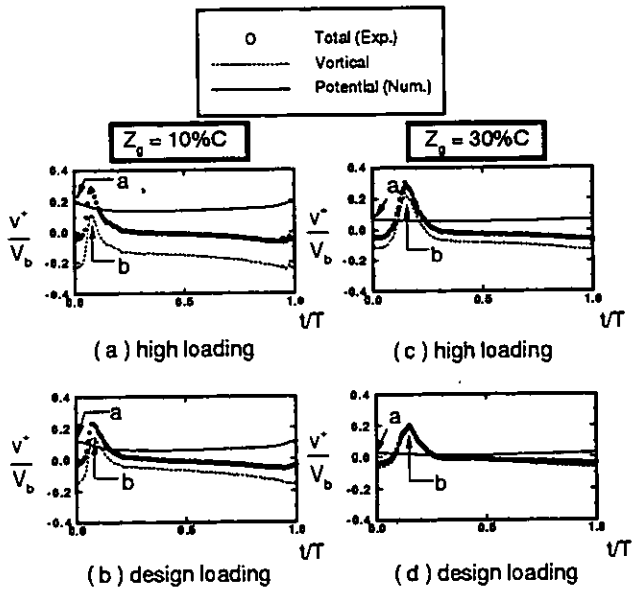

Fig. 9 **Vortical and potential gusts, in the transverse direction, with the hot-wire located at the Point B, see Fig. 8a. The potential gust, from panel calculation, is subtracted from the total gust, measured by the slanted hot-wire, to obtain the vortical gust. Point 'a' when the rotor trailing edge is axially upstream of the probe. Point 'b' corresponds to the time instant when the rotor wake defect arrives at the measurement location.**

potential gusts, in the transverse direction, decomposed using the procedure described in Sec. 4.0. Data were obtained from the hot-wire located at the Point B, at flow conditions near design and at high loadings, and for two axial gap cases. The overall trend is that the vortical gust follows the abrupt increase in the transverse gust, due to a decrease in the axial velocity in the wake, while the potential contribution changes much less severely. The signature of the vortical gust is essentially unchanged for all cases considered, but the potential gust becomes negligible for axial gap of 30%C. This is consistent with the understanding that viscous diffusion is a slow process, which allows many workers to use Euler code to calculate wake/blade interaction (Giles, 1988 and Hall and Crawley, 1989), and that potential disturbance possess an exponential decay characteristics (Manwaring and Wisler, 1993 and Chung and Wo, 1995).

The location 'a' marked in the figures represents the maximum value of the potential gust, which coincides with the time instant when the rotor trailing edge is axially forward of the hot-wire, which is clearly shown in Fig. 8a, for all cases considered. Data with the hot-wire located at Point M also show that the potential gust is largest when the rotor trailing edge is axially upstream of the probe. Thus, we can conclude that for a stationary observer the maximum gust due to potential contribution occurs at the instant when the blade passes.

Similar conclusion can be drawn for the vortical gust. Location 'b' represents the instant when the vortical gust is largest, which occurs at the time when the wake passes the probe, see Fig. 8b. The reason that the time occurrence of location 'a' precedes that of 'b' is mainly due to the rotor stagger angle.

It is desirable to estimate the time when the wake defect, or maximum transverse gust, arrives at the stator leading edge, so that correlation can be made with the time signature of the unsteady force and moment in the next section. To accomplish this, the time that the wake defect passed the Point D was time shifted[4] to the stator leading edge, or to the Point D', with details shown in the enlarged view of Fig. 8a. The Point D was used for this purpose since the wake had already arrived at the suction surface; time shifting the wake defect measured at Point B, or other measurement points, to that of the stator leading edge was found not to provide as good a measure of wake arrival time, since the wake will tend to deform due to the local pressure field near the leading edge.

Figure 10 shows the time shifted wake at the Point D', from the procedure detailed in the footnote. Table 2 summarizes the time when gust reaches a maximum, or when the wake defect passes for gust due to vortical contribution.

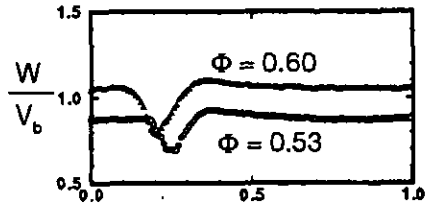

Fig. 10 Wake profile (time shifted) at the Point D', at 10%C axial gap and two time-mean loadings.

Axial Gap	Flow Coefficient(Φ)	Time instant when gust reaches maximum (t/T)			
		Vortical			Potential
		Point B	Point D	Point D'	Point B
10% C	0.53	0.078	0.40	0.24	0.0
	0.60	0.078	0.35	0.19	0.0
30% C	0.53	0.15	N/A	N/A	0.0
	0.6	0.15	N/A	N/A	0.0

Table 2. Time instant when gust reaches a maximum for two axial gaps and time-mean loadings.

[4] The relative position between the Point D and the stator leading edge, or the Point D', is shown in Fig. 8a. This is equivalent to the Point D located at 5.7mm circumferentially above and 1.0mm axially aft of the Point D'. Thus the wake arrives at the Point D' prior to that at the Point D. The procedure requires linear time shifting in the circumferential and axial directions. Time shift in the circumferential direction requires the amount t/T= 5.7mm/43.87mm, or 0.13, where 43.87mm is the rotor pitch, since T is defined by the rotor pitch. Time shift in the axial direction requires the amount t/T= 0.078*1.0mm/3.0mm, or 0.027, where 0.078 is the time when the wake defect arrives at the Point B (see Fig. 9) and Point B is located 3.0mm axially forward of the stator leading edge. From hot-wire data, the wake defect for near design condition, Φ= 0.60, arrives at the Point D at t/T= 0.35. To summarize, the wake defect arrives at the Point D' at t/T= 0.35- 0.13- 0.027= 0.19, which is indicated in Table 2. The same procedure applies for the high loading case, Φ= 0.53.

5.3 Stator Unsteady Force.

Figure 11 shows the stator unsteady force, in the direction normal to the chord, due to vortical, potential, and total contributions, with the total force obtained by integrating the unsteady pressure measured on the stator suction and pressure surfaces at each time instant.

For axial gap of 10%C, Figs. 11a and 11b show that the potential contributed unsteady response reaches a maximum at t/T= 0.0, or when the rotor trailing edge is axially forward of the stator leading edge, see Fig. 8a, which is also when the potential gust maximizes, see Table 2. The potential response is shown to be negligible at 30%C axial gap between rows. The time occurrence of the maxima are summarized in Table 3.

The vortical contributed response dominates the total response, with a clear peak within an unsteady period for design loading, but more broad-band for high loading cases. At axial gap of 10%C, data suggest that larger wake width and defect at high loading cause a greater time lag in the maximum unsteady force.

Axial Gap (Z_g/C)	Flow Coefficient(Φ)	Time reaches maximum (t/T)					
		Vortical			Potential		
		Pt. D'	$\tilde{F}_z$	$\tilde{M}_z$	Pt. B	$\tilde{F}_z$	$\tilde{M}_z$
10%	0.53	0.24	0.35	0.24	0.0	0.0	0.0
	0.60	0.19	0.23	0.22	0.0	0.0	0.0
30%	0.53	N/A	0.42	0.41	0.0	-	-
	0.6	N/A	0.41	0.36	0.0	-	-

Table 3. Time instant when the gust, and unsteady normal force and moment reaches a maximum, for two axial gaps and time-mean loadings.

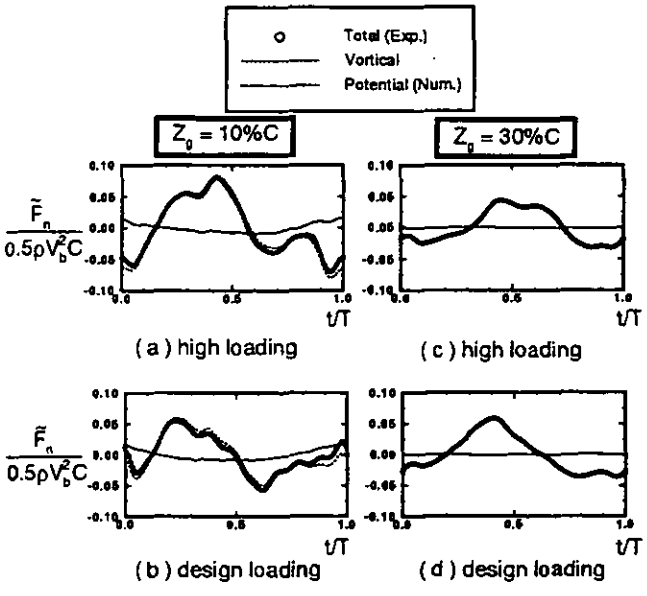

Fig. 11 Excursion of the *unsteady stator response* within a blade-to-blade period, for 10%C and 30%C axial gap cases and at two time-mean loadings. The vortical contributed response dominates and reaches a maximum when the upstream wake arrives near the stator leading edge.

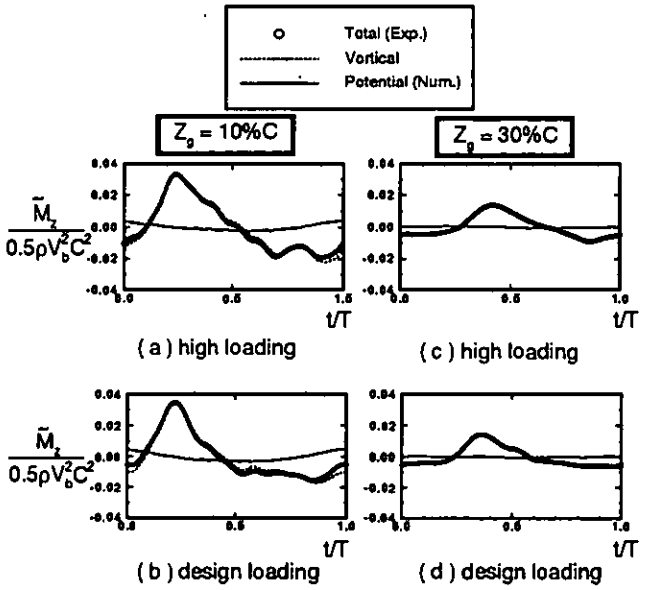

Fig. 12 **Excursion of *unsteady stator moment* about the mid-chord within a blade-to-blade period, for 10%C and 30%C axial gap cases and at two time-mean loadings. The vortical contributed moment dominates and reaches a maximum when the upstream wake reaches the stator leading edge.**

Examination of the unsteady pressure data show the local loading near the leading edge is largest when the wake hits the stator leading edge; the response due to wake impingement dominates the entire unsteady loading. This seems to suggest that wake convection along the blade surface, or motion of the B vortices as described in great detail by Volkov and Tan (1995), is secondary in importance to the effect of wake impingement. They also suggested, correctly, that the impingement process itself is potential in nature, since diffusion of vorticity has not yet acted during the relatively short duration of impingement.

5.4 Stator Unsteady Moment.

Figure 12 shows the stator unsteady moment about the mid-chord in an unsteady period. Figure 12b reveals the moment also maximizes near same instant as the unsteady force in Fig. 11b. The unsteady moment signature also suggests that the wake dominates the entire unsteady process, with the amplitude of the unsteady moment at other time instant to be much smaller. Table 3 also tabulates the time when the peak in the unsteady moment reaches a maximum. Results suggest that, as in the case of the unsteady force, the potential contributed unsteady moment also maximizes when the rotor tailing edge is axially forward of the stator leading edge. The peak due to vortical contribution occurs near the same time instant as the unsteady force, which suggests that maximum bending and torsion are essentially in-phase for the cases studied.

6.0 CONCLUSIONS

This paper studies the unsteady force and moment for a stator in a rotor/stator axial compressor by decomposing the gust and the gust response into vortical and potential contributions. Experiments were conducted in a large-scale, low-speed compressor rig with variable axial gap, at 10% and 30% chord, and at two blade loadings. A 2D Reynolds-averaged Navier-Stokes solver, using disturbance computed by a panel code as an inlet boundary condition, was used to compute the potential contributed response. Major conclusions follows:

- Stator gust response data reveal that the vortical contribution to the unsteady response is largest near the instant when the rotor wake impinges on the stator leading edge.
- The stator unsteady moment, about the mid-chord, also reaches a maximum near the same time instant.
- The potential contributed unsteady response reaches a maximum when the rotor trailing edge is axially upstream of the stator leading edge.
- The vortical contributed response is larger than the potential response for all cases considered, with the potential response negligible at 30%C gap.
- At high loading the unsteady force signature has a broader peak than that near design loading, most likely due to larger wake defect and wake width at high loading.

BIBLIOGRAPHY

Basu, B.C. and Hancock, G.J., 1978, "The unsteady motion of a two dimensional airfoil in incompressible inviscid flow," *J. of Fluid Mechanics*, Vol. 87, pp. 159 - 178.

Chung, M.H., , 1995, "Numerical Study of Vortical and Potential Disturbances and Gust Response in an Axial Compressor," Doctoral thesis (in English), Institute of Applied Mechanics, National Taiwan University.

Chung, M.H. and Wo, A.M., , 1995, "Navier-Stokes and Potential Calculations of Axial Spacing Effect on Vortical and Potential Disturbances and Gust Response in an Axial Compressor," *ASME Paper* 95-GT-301.

Fleeter, S., Jay, R.L. and Bennett, W.A., 1981, "Wake induced time-variant aerodynamics including rotor-stator axial spacing effects," *J. of Fluids Engineering*, Vol. 103, pp. 59 - 66.

Capece, V.R. and Fleeter, S., 1987, "Unsteady Aerodynamic Interactions in a Multistage Compressor," *J. of Turbomachinery*, Vol. 109, pp. 420 - 428.

Gallus, H.E., Grollius, H. and Lambertz, J., 1982, "The influence of blade number ratio and blade row spacing on axial-flow compressor stator blade dynamic load and stage sound pressure level," *J. of Engineering for Power*, Vol. 104, pp. 633 - 641.

Giles, M.B., 1988, "Calculation of unsteady wake/rotor interaction," *J. of Propulsion and Power*, Vol. 4, pp. 356 - 362.

Giles, M.B., 1990, "Stator/Rotor Interaction in a Transonic Turbine," *J. of Propulsion and Power*, Vol. 5, No. 5, pp. 621 - 627.

Hall, K. and Crawley, E., 1989, "Calculation of unsteady flows in turbomachinery using the linearized Euler equations," *AIAA J.*, Vol. 27, No. 6, pp. 777 - 787.

Hobbs, D.E. and Weingold, H.D., 1984, "Development of controlled diffusion aerofoils for multistage compressor applications," *J. Eng. for Gas Turbine & Power*, Vol. 106, pp. 271-278.

Kielb, R.E. and Chiang, H.D., 1992, "Recent advancements in turbomachinery forced response analyses," *AIAA Paper 92-0012*.

Korakianitis, T.P., 1993a, "On the propagation of viscous wakes and potential flow in axial turbine cascades," *J. of Turbomachinery*, Vol. 115, pp. 118 - 127.

Korakianitis, T.P., 1993b, "Influence of stator-rotor gap on axial-turbine unsteady forcing functions," *AIAA J.*, Vol. 31, No. 7, pp. 1256

- 1264.

Kuethe, A.M. and Chow, C.Y., 1986, *Foundations of aerodynamics*, 4th Ed., John Wiley & Sons, Inc., New York, Ch. 5, Sec. 10.

Lamb, H., *Hydrodynamics*, 6th Ed., Dover publications, New York, 1945.

Leonard, B.P., 1979, "A stable and accurate convective modeling procedure based on quadratic upstream interpolation," *Comput. Methods Appl. Mech. Eng.*, Vol. 12, pp. 59-98.

Lewis, J.P. and Delaney, R.A., 1987, "Numerical Prediction of Turbine Vane-Blade Interaction," *AIAA Paper 87-2149*.

Manwaring, S.R. and Wisler, D.C., 1993, "Unsteady aerodynamics and gust response in compressors and turbines," *J. of Turbomachinery*, Vol. 115, pp. 724 - 740.

Morse, A.P., 1991, "Application of a low Reynolds number turbulence model to high-speed rotating cavity flows," *J. of Turbomachinery*, Vol. 113, pp. 98 - 105.

Patankar, S.V. and Spalding, D.B., 1972, "A calculation procedure for heat, mass and momentum transfer in three-dimensional parabolic flows," *Int. J. Heat Mass Transfer*, Vol. 15.

Rai, M.M., 1987, "Navier-Stokes Simulations of Rotor/Stator Interaction Using Patched and Overlaid Grids," *J. of Turbomachinery*, Vol. 112, pp. 377-384.

Rai, M.M. and Madavan, N.K., 1990, "Multi-Airfoil Navier-Stokes Simulations of Turbine Rotor-Stator Interaction," *J. Prapulsian and Power*, Vol. 3, pp. 387-396.

Schmidt, D.P. and Okiishi, T. H., 1977, "Multistage Axial-Flow Turbomachine Wake Production, Transport, and Interation," *AIAA J.*, Vol. 15, No. 8, pp. 1138-1145.

Smith, L.H., 1969, "Casing boundary layers in multistage compressors," *Proceedings of the Symposium on Flow Research on Blading*. Brown Boveri & Co Ltd, Baden, Switzerland. Also in, Dzung, L S (ed) *Flow Research on Blading*. Elsevier Publishing Company 1970.

Valkov, T. and Tan, C.S., 1995, "Control of the Unsteady Flow in a Stator Blade Row Interacting with Upstream Moving Wakes," *J. of Turbomachinery*, Vol. 117, pp. 97 - 105.

Verdon, J.M., 1993, "Review of Unsteady Aerodynamic Methods for Turbomachinery Aeroelastic and Aeroacoustic Applications," *AIAA Journal*, Vol. 31, pp. 235-250.